# FOUR-DIMENSIONAL TRANSVERSE PHASE-SPACE DISTRIBUTION MEASURED BY A PEPPER-POT EMITTANCE METER

T. Nagatomo*, V. Tzoganis[1], M. Kase, O. Kamigaito, and T. Nakagawa,
RIKEN Nishina Center, Wako, Japan
[1]Kockkroft Institute, Warrington, United Kingdom

*Abstract*

In this study, we observed variations in the four-dimensional transverse emittance, $\epsilon_{4D}$, of argon beams having several charge states with respect to the amount of residual gas in the low-energy beam transport (LEBT) of a 18-GHz superconducting electron cyclotron resonance ion source (18-GHz SC-ECRIS) at RIKEN, as measured by a pepper-pot emittance meter. Natural krypton gas was injected into the LEBT to control the amount of residual gases. Collisions between the beams and the residual gaseous atoms generated electrons that were expected to cancel out the positive electric potential inside the beam, or, in other words, achieve space-charge compensation. Reductions in the emittance of $^{40}Ar^{8+}$, $^{9+}$ and $^{11+}$ beams were observed by the injection of krypton gas into the LEBT. The reductions in projected emittances such as $\epsilon_x$ and $\epsilon_y$ were different for each charge state; however, the reduction in $\epsilon_{4D}$ of these charge states were similar to each other. The degree of reduction in $\epsilon_{4D}$ was about 50% when the residual gas pressure of the LEBT was changed from $1.9\times10^{-7}$ mbar to $1.3\times10^{-5}$ mbar. The mechanism of the reduction in emittance is not clarified in this paper because there is a possibility that the reduction was caused by the change in electron cyclotron resonance plasma, which is induced by the penetration of the injected krypton gas into the plasma chamber.

## INTRODUCTION

Recently, the importance of the emittance of four-dimensional (4-D) phase space, $\epsilon_{4D}$, has received much attention, and it has been discussed with the aim of improving beam quality [1–3]. $\epsilon_{4D}$ is an invariant under linear 4-D symplectic transformation, such as beam transport using linear optical components including solenoid and skew-quadrupole lenses. On the other hand, the two-dimensional (2-D) emittances, $\epsilon_x$ and $\epsilon_y$, are not invariant when a solenoid lens or a skew-quadruple lens are used because both types of lenses can couple these quantities. If there is no acceleration/deceleration, no beam loss, and no non-linear effects, $\epsilon_{4D}$ should remain constant during beam transport. Thus, measurement of $\epsilon_{4D}$ provides quantitative and essential information that can be used to improve beam quality in the real sense of the term.

As is well known, attention must be paid to any aberrations in the beam optics components and the space-charge effect when the ion-beam current is high, as these degrade the beam quality through the enhancement of the beam emittance. The possibility of space-charge compensation by a deliberate injection of a neutral gas into the LEBT was discussed by Toivanen et al. [4]. Based on that report, we have developed an on-line pepper-pot emittance meter that is suitable for obtaining $\epsilon_{4D}$ [5], and studied how the $\epsilon_{4D}$ of multiply charged argon beams evolves with respect to the amount of neutral krypton gas injected in the LEBT. We report some preliminary, but interesting, trends in these emittances.

## EXPERIMENTAL SETUP

### *Pepper-pot Emittance Meter*

The pepper-pot emittance meter consists of a thin metallic plate (50 μm thick) with a 25 × 25-pinhole array and an imaging screen to detect transverse deviation of the beamlets. The diameter of each pinhole is 0.1 mm, and the pitch of the pinholes is 2.0 mm in both the horizontal and vertical directions. An imaging screen (P46) was placed behind a microchannel plate (MCP) that was employed to convert the heavy ions into electrons in order to prolong the lifetime of the screen. The pinhole plate was translated along the beam axis using a stepper motor to find the optimum distance between the pinhole plate and the MCP. The distance could be varied from 23 mm to 56 mm, and was calibrated with respect to the number of electric pulses driving the stepper motor. The beamlet image reflected by a mirror angled at 45 degrees was detected through a viewport by a CMOS camera. An electrical beam chopper placed in front of the emittance meter was synchronized with the CMOS camera to stop the beam when images were not being acquired. For more details of the mechanical design, please refer to [5].

We also developed image-capture and emittance-analysis programs using LabVIEW (National Instruments Co.). We programmed a process that automatically identifies the correspondence between each of the beam spots and the pinhole through which the beamlet passed. It is possible to obtain the particle distribution in 4-D transverse phase-space from this analysis. Therefore, from the distribution in the 4-D phase space, $(x, x', y, y')$, six types of two-dimensional projections can be generated, i.e. $x$-$x'$, $y$-$y'$, $x$-$y$, $x'$-$y'$, $x$-$y'$ and $y$-$x'$ projections. The developed program displays all the projected distributions simultaneously, as shown in Fig. 1, immediately after the beamlet image is captured. In addition, the $\epsilon_{4D}$, the transverse beam matrix $C$ and the two-dimensional emittances, which are described in the following section, are also calculated and displayed. All of these processes, including the image-capture process, can be com-

* email nagatomo@riken.jp



ISBN 978-3-95450-186-1

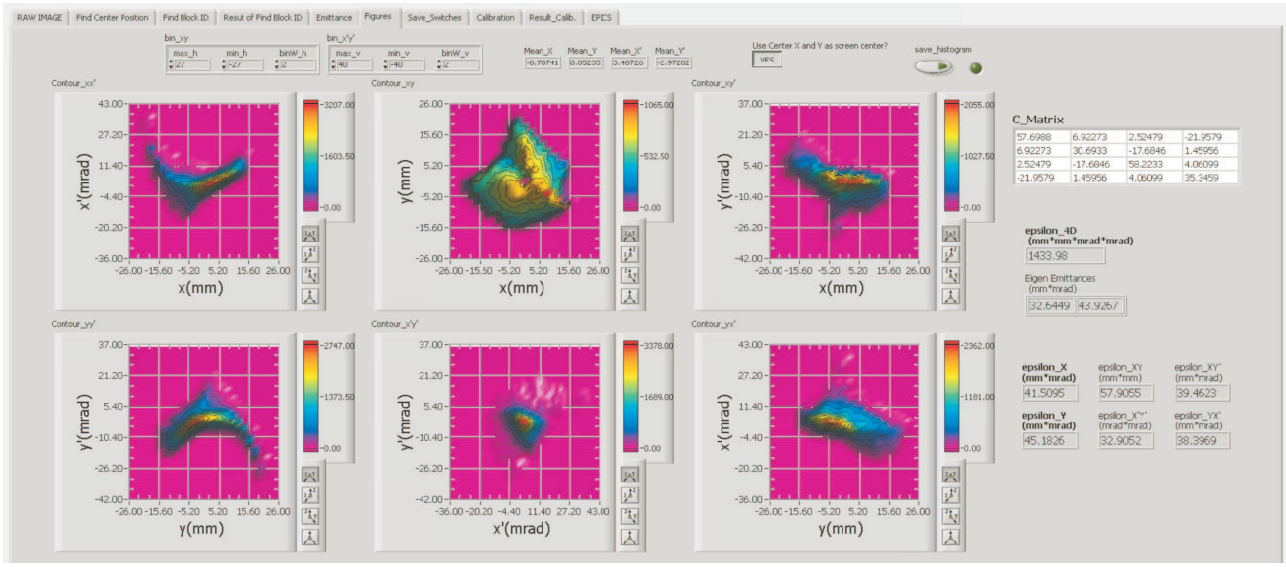


Figure 1: Typical screenshot of the developed on-line emittance monitor. This program displays six types of 2-D distributions together with the quantities of $\epsilon_{4D}$, the 2-D emittances and the transverse beam matrix $C$.

pleted within one second, which is quick enough to enable this system to be used as an on-line emittance monitor.

### *RIKEN 18-GHz SC-ECR Ion Source and LEBT*

The layout of the RIKEN 18-GHz Superconducting ECR Ion Source (18-GHz SC-ECRIS) together with the LEBT is shown in Fig. 2. The LEBT consists of an analyzing magnet, an electric beam chopper, a diagnostics chamber, a solenoid lens, and a pepper-pot emittance meter. An Einzel lens and two xy steering magnets are included in the setup; however, they were turned off during the measurements. A Faraday cup in a diagnostics chamber was used to measure the beam current with a set of horizontal and vertical slits (XY slits) fully opened as ±20 mm. The emittance meter described in the previous section was installed behind the solenoid lens.

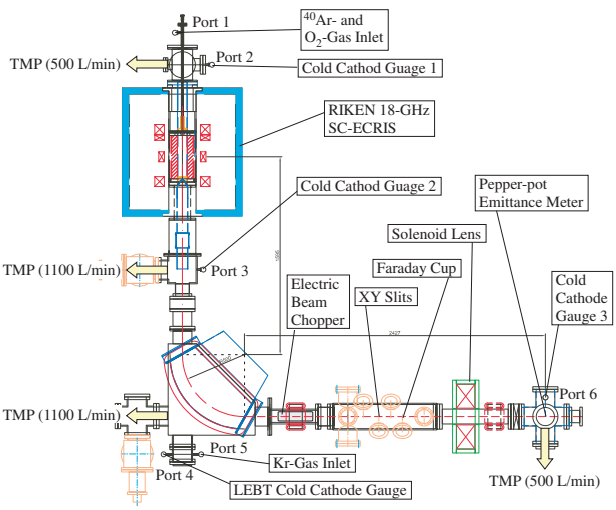


Figure 2: Schematic layout of the 18-GHz SC-ECRIS and LEBT.

The multiply charged argon beams were generated by the 18-GHz SC-ECRIS. A mixture of argon and oxygen gases was fed into a plasma chamber through Port 1 in Fig. 2, and the oxygen gas was employed as a support gas to optimize the argon beam by the gas mixing method. The flow rate of each gas was controlled using a precision variable leak valve. The ion-extraction voltage was set to 10.0 kV for all charge states. The parameters of the ECRIS, such as the microwave power of 680 W, the argon and oxygen flow rates, the mirror field, the position of a biased disk inside the plasma chamber, the voltage applied on the biased disk were adjusted in order to optimize the current of the $^{40}Ar^{11+}$ beam at the Faraday cap after the analyzing magnet, prior to the injection of krypton gas mentioned below. The ion-source parameters were kept constant during all measurements.

Natural krypton gas was injected through a precision variable leak valve attached to Port 5 in Fig. 2, which is located behind the analyzing magnet. Krypton was selected because the first ionization is slightly smaller than that of argon and nitrogen atoms, and is comparable to that of oxygen. The residual gas pressure of the LEBT was monitored using a cold cathode gauge (CCG) attached to Port 4, which is adjacent to Port 5 used for gas injection. In addition, CCGs 1–3 were attached to Ports 2, 3 and 6, respectively, to monitor the diffusion of the injected krypton gas. The LEBT residual gas pressure was controlled from $1.9 \times 10^{-7}$ mbar to $1.3 \times 10^{-5}$ mbar using the leak rate of the krypton gas.

We chose the $^{40}Ar^{8+,9+}$ and $^{11+}$ beams for the emittance measurements, and the magnetic fields of the analyzer magnet and the solenoid lens were tuned to the $B\rho$ for each beam. By measuring the beam current and 4-D phase-space distribution using the Faraday cup and the pepper-pot emittance meter, respectively, we studied how beam intensity and not only the projected emittances $\epsilon_x$ and $\epsilon_y$, but also $\epsilon_{4D}$ varied along with the LEBT gas pressure.

ISBN 978-3-95450-186-1

## RESULTS AND DISCUSSIONS

### *Definition of Emittance*

As described in Refs. [1–3], the 4-D (rms) emittance $\epsilon_{4D}$ is determined by the transverse beam matrix $C$ as:

$$\epsilon_{4D} = \sqrt{detC}, \tag{1}$$

where

$$C = \begin{pmatrix} \langle xx \rangle & \langle xx' \rangle & \langle xy \rangle & \langle xy' \rangle \\ \langle x'x \rangle & \langle x'x' \rangle & \langle x'y \rangle & \langle x'y' \rangle \\ \langle yx \rangle & \langle yx' \rangle & \langle yy \rangle & \langle yy' \rangle \\ \langle y'x \rangle & \langle y'x' \rangle & \langle y'y \rangle & \langle y'y' \rangle \end{pmatrix}. \tag{2}$$

The (rms) emittance projected into a 2-D phase space is determined as the square root of the determinant of a submatrix of $C$, for example:

$$\epsilon_x = \sqrt{detC_{xx'}} \text{ with } C_{xx'} = \begin{pmatrix} \langle xx \rangle & \langle xx' \rangle \\ \langle x'x \rangle & \langle x'x' \rangle \end{pmatrix}. \tag{3}$$

In the 2-D phase space, the area surrounded by the rms ellipse, $S$, is described as the product of its emittance value and $\pi$, for example, $S_x = \pi \times \epsilon_x$.

The following expression between $\epsilon_x$, $\epsilon_y$ and $\epsilon_{4D}$ is established:

$$\epsilon_{4D} \leq \epsilon_x \epsilon_y, \tag{4}$$

with equality if there is no inter-plane correlation.

### *Changes in Beam Current and Mmittance*

The beam currents, the 2-D emittances, $\epsilon_x$ and $\epsilon_y$, and the 4-D emittance $\epsilon_{4D}$ are obtained with respect to the residual gas pressure of LEBT, as shown in Fig. 3. The $^{40}Ar^{9+}$- and $^{40}Ar^{11+}$-beam currents begin to decrease at an LEBT pressure of $\sim 2.5 \times 10^{-6}$ mbar. On the other hand, the $^{40}Ar^{8+}$-beam current begins to increase rapidly around $1.0 \times 10^{-6}$ mbar. These decreases (increases) in beam current for higher (lower) charge states are caused by a charge exchange between the argon beam and neutral krypton gas occurring during beam transport, and/or the charge distribution of the ECR plasma being changed, as discussed in the following section.

Focusing on the 2-D emittance, both $\epsilon_x$ and $\epsilon_y$ gradually decrease as the LEBT gas pressure increases; however, the degree of the reduction of $^{40}Ar^{11+}$ is quite different from that of the others, as shown in Fig. 3. In Fig. 3, each emittance is normalized by a value obtained in a case where there is no krypton-gas injection, and these values are listed in the figure. Compared to the value obtained in the case where there is no gas injection, $\epsilon_x(\epsilon_y)$ of $^{40}Ar^{11+}$ decreases by 9%(14%) at $1.3 \times 10^{-5}$ mbar. On the other hand, in the case of $^{40}Ar^{9+}$, $\epsilon_x$ ($\epsilon_y$) decreases by 32% (33%), and in the $^{40}Ar^{8+}$ case, $\epsilon_x$ ($\epsilon_y$) decreases by 26% (44%). Note that in the case of a charge state of 8+, despite the fact that the beam current increases by a factor of about two, both $\epsilon_x$ and $\epsilon_y$ decrease by about one third, and this indicates that the beam brightness of $^{40}Ar^{8+}$ is improved by the injection of krypton gas.

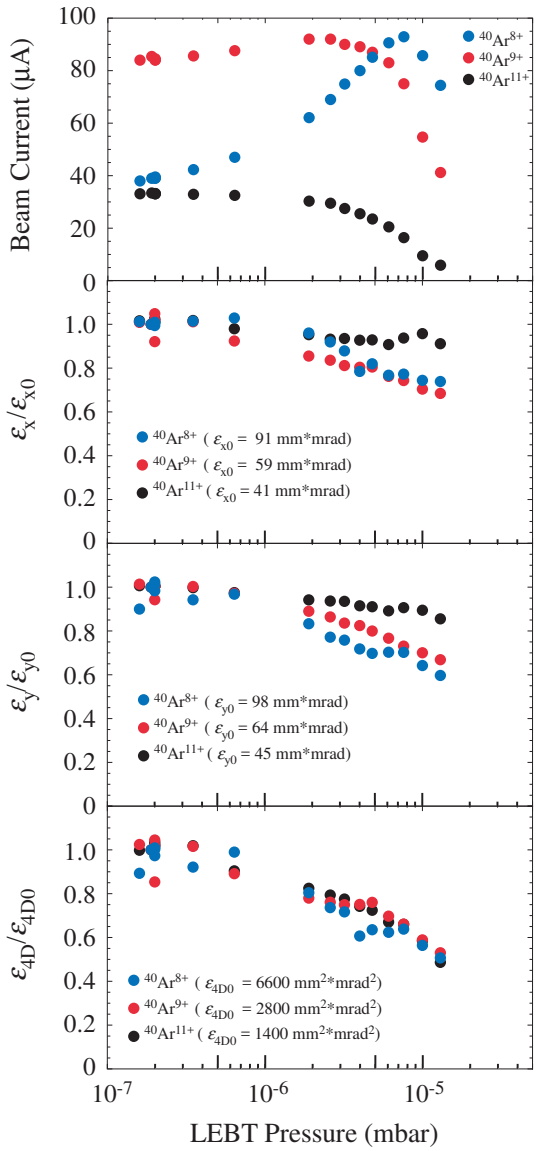


Figure 3: Obtained beam currents and rms emittances $\epsilon_x$, $\epsilon_y$ and $\epsilon_{4D}$ of $^{40}Ar^{8+,9+}$ and $^{10+}$ with respect to the LEBT residual gas pressure. For each charge state, these emittances were normalized by the values obtained under the condition of no Kr-gas injection, $\epsilon_{x0}$, $\epsilon_{y_0}$ and $\epsilon_{4D0}$, respectively.

Furthermore, focusing on the 4-D emittance, the $\epsilon_{4D}$ of $^{40}Ar^{8+,9+}$ and $^{11+}$ seem to decrease similar to each other, despite the fact that its projections in the 2-D phase space, $\epsilon_x$ and $\epsilon_y$, are different from each charge state. Compared to the value for the no-gas injection case, the amount of the reduction is about 50 % at $1.3 \times 10^{-5}$ mbar for each charge state.

At present, we cannot clearly describe the mechanism that causes these emittance reductions, because we cannot distinguish the effects of the LEBT, e.g., the reduction of the beam-optics aberrations and reduction of the space-charge, from the effect caused by the changes in the electron cy-



ISBN 978-3-95450-186-1

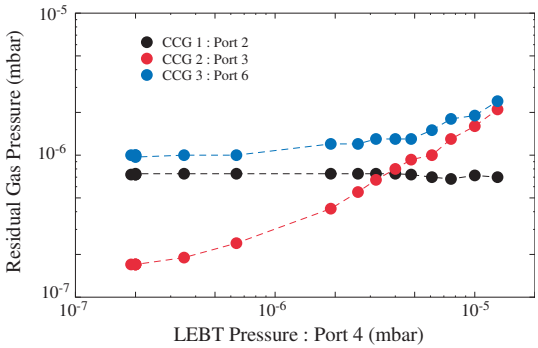


Figure 4: Residual gas pressure measured by cold cathode gauges CCGs 1–3 attached to Ports 2, 3 and 6, respectively, in Fig. 2. The residual gas pressure was expressed as a function of the LEBT residual gas pressure measured at Port 4 adjacent to the site of Kr-gas injection.

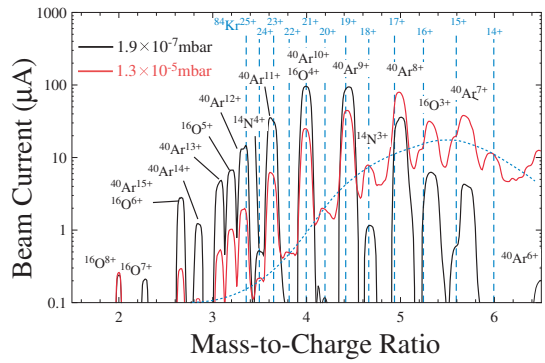


Figure 5: Charge distributions obtained at a residual LEBT gas pressure of $1.9 \times 10^{-7}$ and $1.3 \times 10^{-5}$ mbar, shown as black and red lines, respectively. Blue dashed lines indicate the mass-to-charge ratios of $^{84}$Kr beams. The peaks of $^{84}$Kr located between $^{40}$Ar and $^{16}$O peaks are smoothly connected, as shown using a blue dotted line to guide the eye.

clotron resonance (ECR) plasma as discussed in the following section. A complementary experiment to distinguish these effects is therefore required to clarify the emittance-reduction mechanism.

### *Possible Change in ECR Plasma*

It is easily seen from Fig. 2 that the injected krypton gas was diffused into not only all areas of the LEBT but also the plasma chamber in which the ion beams are generated. Thus, we have to pay attention to the possibility of a change in the ECR plasma conditions caused by the penetrating krypton gas. Figure 4 shows the change in residual gas pressure measured by the CCGs installed at several points, as shown in Fig. 2. Two vacuum chambers, an upstream chamber and downstream chamber, the pressures of which are monitored by CCG1 and CCG2, respectively, sandwich the plasma chamber, and these chambers are connected to each other. The injected krypton gas penetrates from downstream into these chambers. As shown in Fig. 4, at an LEBT pressure of around $3.0 \times 10^{-6}$ mbar, the vacuum levels of the upstream and downstream chambers are identical. Furthermore, at an LEBT pressure greater than $3.0 \times 10^{-6}$ mbar, the magnitude relation of the vacuum levels of these chambers is reversed, which means that the amount of krypton gas that penetrated into the plasma chamber is not negligible.

Figure 5 shows the charge distributions of the extracted ion beams at an LEBT pressure of $1.9 \times 10^{-7}$ mbar (no-krypton injection) and $1.3 \times 10^{-5}$ mbar by a solid black line and a solid red line, respectively, together with the positions of mass-to-charge ratio of $^{84}$Kr ions. We can clearly see several $^{84}$Kr peaks between $^{40}$Ar and/or $^{16}$O peaks at $1.3 \times 10^{-5}$ mbar, which vanish at $1.9 \times 10^{-7}$ mbar. We can roughly estimate that the amount of Kr is about one order of magnitude smaller than that of Ar for each of the charge states of 8+, 9+ and 11+, taking the height of these clear $^{84}$Kr peaks and the difference in the mass-to-charge ratio into account. However, the ECR plasma should be affected by the gas-mixing effect induced by the penetrating krypton.

In addition, note that the charge distribution shown in Fig. 5 was obtained after the analyzing magnet, which means that the obtained charge distribution includes both the effects of the change in ECR-plasma and the charge exchange effects during beam transport. Thus, further studies are required.

In a future study, we plan to inject krypton gas into Port 1 in Fig. 2, which is used for the injection of the argon and oxygen gases. After reconstruction of the charge distribution shown in Fig. 5, we will reinvestigate how the $\epsilon_{x,y}$ and $\epsilon_{4D}$ depends on the LEBT residual gas pressure or the extracted beam currents to distinguish the effects caused by the residual gas in the LEBT from the state of the ECR plasma.

## REFERENCES

[1] L. Groening, "Concept for controlled transverse emittance transfer within a linac ion beam," *Phys. Rev. ST Accel. Beams*, Vol. 14, pp. 064201, Jun. 2011.

[2] C. Xiao *et al.*, "Single-knob beam line for transverse emittance partitioning," *Phys. Rev. ST Accel. Beams*, Vol. 16, pp. 044201, Apr. 2013.

[3] C. Xiao *et al.*, "Rotating system for four-dimensional transverse rms-emittance measurements," *Phys. Rev. ST Accel. Beams*, Vol. 19, pp. 072802, Jul. 2016.

[4] V. Toivanen *et al.*, "The effects of beam line pressure on the beam quality of an electron cyclotron resonance ion source," *Nucl. Instr. Meth. B*, Vol. 268, pp. 1508–1516, 2010.

[5] V. Tzoganis *et al.*, in *Proc. 7st Int. Particle Accelerator Conf. (IPAC'16)*, Busan, Koria, May 2016, paper MOPMR048, pp. 361–363.



ISBN 978-3-95450-186-1